Microsyst Technol (2012) 18:1267–1281
DOI 10.1007/s00542-012-1518-9

TECHNICAL PAPER

Maximum power tracking of a generic photovoltaic system via a fuzzy controller and a two-stage DC–DC converter

Paul C.-P. Chao · Wei-Dar Chen · Chih-Kuo Chang

Received: 30 September 2011 / Accepted: 23 April 2012 / Published online: 9 May 2012

Abstract This study presents a new two-stage DC–DC converter for maximum power point tracking (MPPT) and a voltage boost of a generic photovoltaic (PV) system. An intelligent MPPT of PV system based on fuzzy logic control (FLC) is presented to adaptively design the proposed fuzzy controlled MPPT controller (FC-MPPTC) while a voltage boost controller (VBC) is used to fix the output voltage to a voltage level that is higher than the required operating voltage to the back-end grid impedance. Modeling and simulation on the PV system and the DC–DC converter circuit are achieved by state-space and the software Powersim. The PV string considered has the rated power around 600 VA under varied partial shadings. The FC-MPPTC and VBC are designed and realized by a DSP module (TMS320F2812) to adjust the duty cycle in the two-stage DC–DC converter. A special FLC algorithm is forged to render an MPPT faster and more accurate than conventional MPPT technique, perturb and observe (P&O). The simulations are intended to validate the performance of the proposed FC-MPPTC. Experiments are conducted and results show that MPPT can be achieved in a fast pace and the efficiency reaches over 90 %, even up to 96 %. It is also found that the optimized tracking speed of the proposed FC-MPPTC is in fact more stable and faster than the general P&O method with the boost voltage capable of offering a stable DC output.

P. C.-P. Chao (✉) · W.-D. Chen · C.-K. Chang
Department of Electrical Engineering, National Chiao Tung University, Hsinchu 300, Taiwan
e-mail: pchao@mail.nctu.edu.tw

P. C.-P. Chao
National Chiao Tung University, Institute of Imaging and Biomedical Photonics, Tainan 711, Taiwan

1 Introduction

Emission of carbon dioxide is commonly regarded nowadays as a major obstacle toward a clean world, thus clean energies other than fossil fuel are intensively sought recently by academic societies and industry. Renewable energies have, as one of clean energies, become one viable candidate to replace traditional fossil fuel. Renewable energy comes from natural resources, such as wind power energy, hydro energy, biomass energy, geothermal energy, ocean energy and photovoltaic (PV) energy. Among aforementioned renewable energies, the photovoltaic (PV) energy is expected to be a major clean energy source without pollution and energy waste due to accessibility of solar energy and relative simplicity involved in the manufacture, structure and electronics of a PV array.

In a typical PV system, there is usually a DC–DC converter (Mohan 1995), which is designed responsible for driving power out of the front-end PV panel. The function of this DC–DC converter is to adjust its impedance seen by the PV panel to be close to the corresponding impedance of the PV panel, thus maximizing the output efficiency. The combination of corresponding current and voltage of the PV panel is so-called the maximum power point (MPP) in the characteristic curve-voltage curves. The adjustment of the impedance is made possible via a power switch in the DC–DC converter, the duty cycle of which can actively adjusted by an external controller. A number of past research works have been devoted to design controllers for the on-line tracking of MPP (maximum power point tracking, MPPT), either using a classic or advanced controller (Yuvarajan et al. 2004; Zhong et al. 2008; Xiao et al. 2007). One of most difficult tasks for these controllers is to be adjusted to varied conditions of solar irradiation, shading and external temperature that may result in significant changes in the current–

voltage characteristics curves (I–V curves) of a PV array, leading to different locations of MPP. Thus, an on-line tracking scheme for MPP is necessary in order to keep the operation of the PV panel constantly at MPP (Gao 2009; Win et al. 2011). Many methods and controllers have been developed to track the MPP like as methods of power feedback control (Al-Atrash et al. 2005), perturb and observe (P&O) (Santos et al. 2006; Hua et al. 1998; Jiang et al. 2005) or incremental conductance (Hussein et al. 1993; Wasynczuk 1983). These control schemes suffer different drawbacks during MPPT; for instance, the P&O has oscillation problem. Therefore, other intelligent control methods like fuzzy logic or neural network were introduced in (Kottas et al. 2006; Chiu 2010; Agorreta et al. 2009; Bouchafaa et al. 2011; Salah and Ouali 2011).

Due to the constant variation in the I–V characteristics curves of a PV panel in realistic operations, the output voltage of the DC–DC converters under MPPT operation may vary in a wide range. It is thus possible that the output voltage is below the required input voltage level to the subsequent inverter and/or grid (e.g. in dark environment), resulting in a great difficulty in power transfer. To remedy the problem, another stage of DC–DC boost converter is add in this study before the inverter and/or grid to perform the power conditioning for providing electric power in high voltage levels. The entire circuit topology becomes a two-stage power conversion circuit.

A fuzzy controlled MPPT (FC-MPPTC) controller for the first stage and a voltage boost controller (VBC) for the second stage are designed in this study for both fast maximum power tracking and high conversion efficiency. The MPPT controller is used for maximum power transfer, while the VBC is to boost the output voltage above the operable voltages of the back-end electronics (e.g. inverter and/or grid) (SMA Solar Technology 2010). Note that the duty-tunings by the two independent controllers in the proposed two-stage converter are able to tackle both fast-changing front-end PV conditions and back-end impedance, simultaneously. To design the fuzzy MPPT controller and also determine the duty-tuning schemes for the two stages, a state-space dynamic model in terms of average current is first established, followed by Powersim simulation. The performance of the designed fuzzy MPPT and duty-tuning schemes are evaluated by simulations. With satisfactory simulated performance, experiments are next conducted for validation. It is shown that the resulted experimental efficiency is up to 96 %, which is obviously difficult to achieve by a single-stage converter if the I–V characteristics curves vary constantly due to the changes in external conditions, like shading and temperature, etc.

The remainder of this study is organized as follows. Section 2 analyzes and establishes a state-space model for the PV array, which is followed by determination of passive components used in the two-stage converter. Section 3 provides the design processes and details of the FC-MPPTC controller. In Sect. 4, the performance of designed system is simulated by Powersim to confirm the effectiveness of the designed FC-MPPTC controller in enabling a fast and smooth MPPT. Experimental setup and results are also given in this section to validate the controller performance. Finally, Sect. 5 provides brief concluding remarks and intended directions for future research work.

2 System and modeling and design

2.1 System description

A two-stage photovoltaic (PV) system shown in Fig. 1 is considered in this study. The system is supposed to consist of a PV array and a two-stage boost converter. The power switches of the system are controlled by the gate drivers programmed via a DSP module. The converter delivers required levels of power output to the rear-end power grid. The impedance of the power grid would be assumed as suitable ones for subsequent analysis in this study. The first and second stages of the two-stage converter are responsible for MPPT and voltage regulation, respectively. The equivalent circuit of the considered PV array is shown in Fig. 2, where the PV array is modeled by a parallel connection of a current source I_{PH}, a diode, an internal parallel and series resistances, R_{SH} and R_S. The relationship between the current and the voltage of the PV array V_{pv} can be well prescribed by (Kwon et al. 2006).

$$I_{pv} = I_{PH} - I_s\left[\exp\left(\frac{q(V_{pv} + I_{pv}R_s)}{AKT}\right) - 1\right] - \frac{V_{pv} + I_{pv}R_s}{R_{SH}}, \tag{1}$$

where I_{pv} is the output current of the PV array; I_s is the saturation current; q is the charge of an electron; K is the Boltzmann's constant; A is the ideality factor of the p–n junction; T is the temperature (deg K) of the PV array. The irradiation and temperature influence the output power in a nonlinear relation at every moment. The characteristics curves for I–V and P–V relations of the PV array (Siemens solar module SP75 is considered) can be simulated by a commercial software Powersim with Eq. (1). Figure 3 displays the simulation results for different energy densities and temperatures of a PV array. It is evident from this figure that under the different irradiation and temperature conditions, the maximum power pint (MPP) is changed. It means that the MPP is a time-vary parameter. This makes the maximum power point tracking (MPPT) a difficult task.

Various techniques to achieve an on-line, dynamic MPPT have been reported by researchers. The most common one is the Perturb and Observation (P&O) method

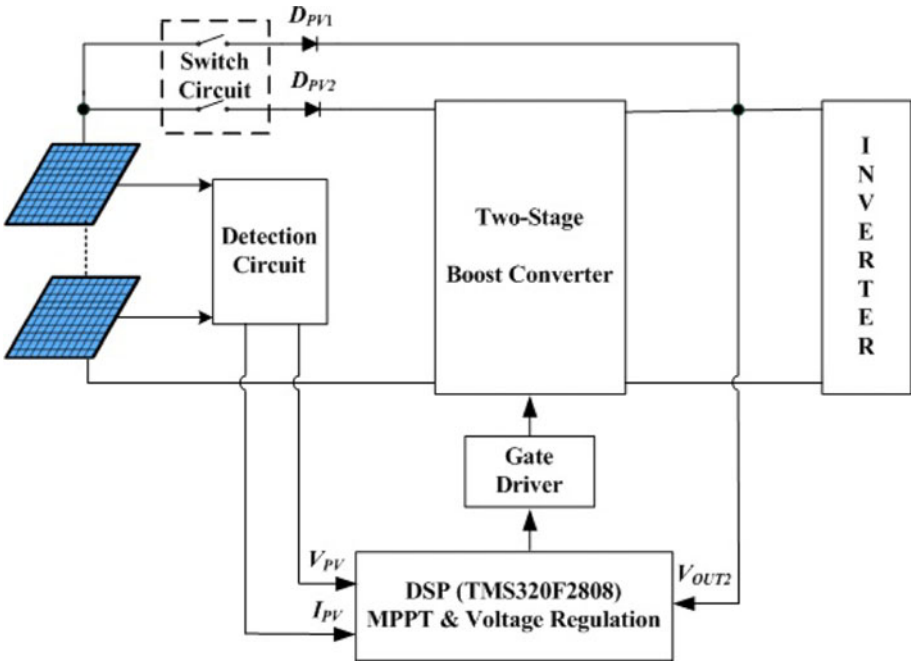

Fig. 1 The two-stage PV system

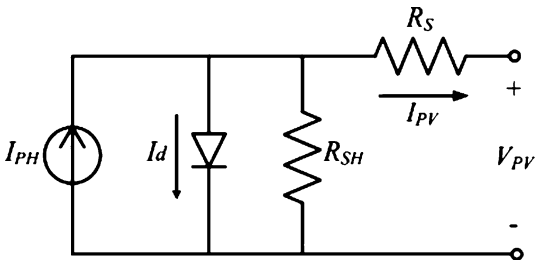

Fig. 2 The equivalent circuit of the PV array

(Santos et al. 2006; Hua et al. 1998; Jiang et al. 2005), due to its simplicity and ease to achieve MPPT. The method proposes four simple tuning rules on the duty for different polarity combinations of changes in power and voltage of the PV array. The tuning increment on the duty is however fixed. Therefore, the time span required to reach MPPT is relatively long, not to mention the difficulty for the tracker to stay right on the MPP since each time the perturbation on tuning the voltage is finite. To tackle the aforementioned disadvantage, some intelligent control methods were developed recently (Kottas et al. 2006; Chiu 2010; Agorreta et al. 2009; Bouchafaa et al. 2011; Salah and Ouali 2011). In this study, a fuzzy logic controller (FLC) is designed, which make possible a varying increment for the output duty. The increment is determined by the fuzzy mechanism. This aims to realize a fast, smooth and accurate MPPT. The designed FLC control algorithm consists mainly of four parts as shown in Fig. 4. The input signals experiences fuzzification, interference rules and finally defussification. The interference rules could follow the same deterministic rules adopted by the conventional P&O method, a flow-chart representation of which is given in Fig. 5. The design details of the FC-MPPTC controller is given in Sect. 3.

2.2 Modeling on the two-stage DC–DC converter

The topology of a two-stage DC–DC converter, as shown in Fig. 6, is adopted in this study for simultaneous MPPT and boosting the output voltage to a required higher level A subsequent DC–AC inverter for converting the power to grid is supposed to be connected to the rear end of the converter. The duty cycle of the switch Q_1 for the first stage is adjusted by the designed fuzzy logic control for MPPT, while that of the switch Q_2 for the second stage is adjusted for boosting the output voltage to a required DC level for the subsequent inverter and gird.

To model the electrical dynamics of the converter for two stages, two different switching conditions as shown in Fig. 7 for the MOSFET Q_1 and Q_2 in Fig. 6 have to be considered. They results in different sets of governing equations in state-space forms. In case I, the duty cycle of Q_1 is longer than Q_2, while for case II the duty cycle of Q_1 is shorter than Q_2. The whole switching period can be divided into three different parts, D_1 (D'_1), D_2 (D'_2) and $1 - D_1 - D_2$ ($1 - D'_1 - D'_2$). In the period of D_1, Q_1 and Q_2 are both on. In the period of D_2, only one of Q_1 and Q_2 is on. In the period of $(1 - D_1 - D_2)$, Q_1 and Q_2 are both off. The time evolutions of all capacitance currents and inductance voltages for the three periods in case I can be derived by Kirchhoff's current law (KCL) and Kirchhoff's voltage law (KVL) in the converter topology shown in Fig. 6. The derivation results are expressed in terms of state-space form as below,

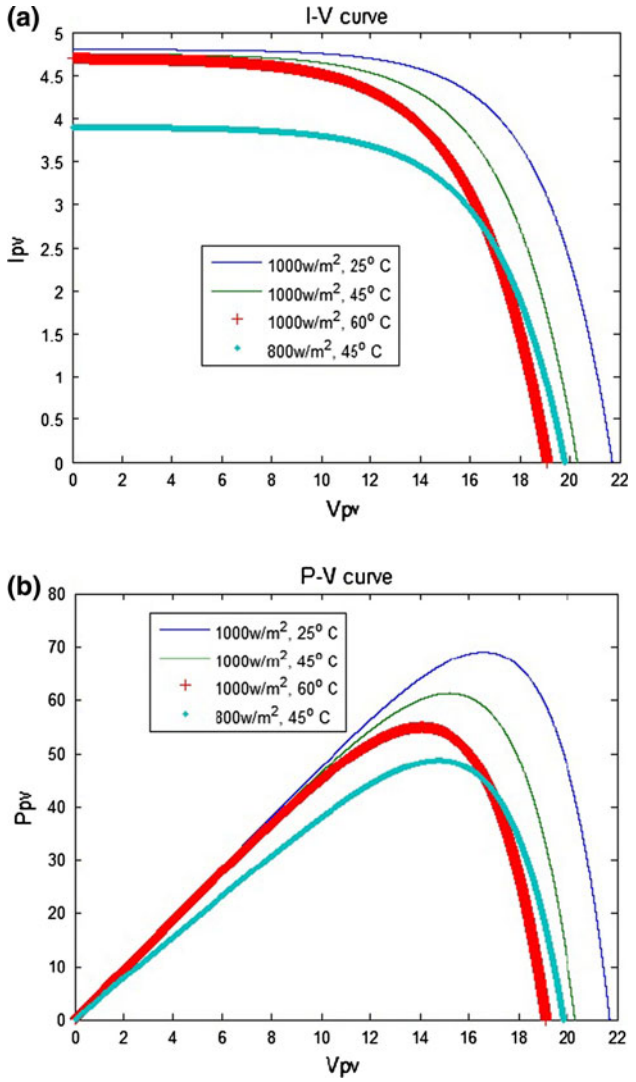

Fig. 3 **a** I–V curve and **b** P–V curve of PV array

$$\begin{bmatrix} \dot{i}_{L1}(t) \\ \dot{i}_{L2}(t) \\ \dot{V}_{C1}(t) \\ \dot{V}_{C2}(t) \end{bmatrix} = \begin{bmatrix} 0 & 0 & 0 & 0 \\ 0 & 0 & \frac{D_1}{L_2} & 0 \\ 0 & \frac{-D_1}{C_1} & 0 & 0 \\ 0 & 0 & 0 & \frac{-D_1}{R_L C_2} \end{bmatrix} \begin{bmatrix} i_{L1}(t) \\ i_{L2}(t) \\ V_{C1}(t) \\ V_{C2}(t) \end{bmatrix} + \begin{bmatrix} \frac{D_1}{L_1} \\ 0 \\ 0 \\ 0 \end{bmatrix} V_{PV}(t), \tag{2}$$

$$\begin{bmatrix} \dot{i}_{L1}(t) \\ \dot{i}_{L2}(t) \\ \dot{V}_{C1}(t) \\ \dot{V}_{C2}(t) \end{bmatrix} = \begin{bmatrix} 0 & 0 & 0 & 0 \\ 0 & 0 & \frac{D_2}{L_2} & \frac{-D_2}{L_2} \\ 0 & \frac{-D_2}{C_1} & 0 & 0 \\ 0 & \frac{D_2}{C_2} & 0 & \frac{-D_2}{R_L C_2} \end{bmatrix} \begin{bmatrix} i_{L1}(t) \\ i_{L2}(t) \\ V_{C1}(t) \\ V_{C2}(t) \end{bmatrix} + \begin{bmatrix} \frac{D_2}{L_1} \\ 0 \\ 0 \\ 0 \end{bmatrix} V_{PV}(t), \tag{3}$$

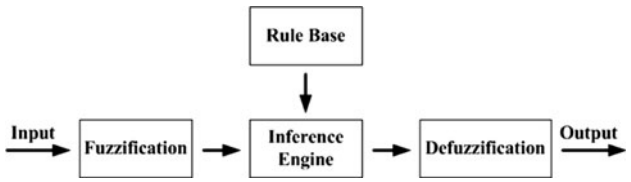

Fig. 4 The computation required for FLC

$$\begin{bmatrix} \dot{i}_{L1}(t) \\ \dot{i}_{L2}(t) \\ \dot{V}_{C1}(t) \\ \dot{V}_{C2}(t) \end{bmatrix} = \begin{bmatrix} 0 & 0 & \frac{-(1-D_1-D_2)}{L_1} & 0 \\ 0 & 0 & \frac{1-D_1-D_2}{L_2} & \frac{-(1-D_1-D_2)}{L_2} \\ \frac{1-D_1-D_2}{C_1} & \frac{-(1-D_1-D_2)}{C_1} & 0 & 0 \\ 0 & \frac{1-D_1-D_2}{C_2} & 0 & \frac{1-D_1-D_2}{R_L C_2} \end{bmatrix} \times \begin{bmatrix} i_{L1}(t) \\ i_{L2}(t) \\ V_{C1}(t) \\ V_{C2}(t) \end{bmatrix} + \begin{bmatrix} \frac{1-D_1-D_2}{L_1} \\ 0 \\ 0 \\ 0 \end{bmatrix} V_{PV}(t), \tag{4}$$

where D_1 is the duty cycle of part I; D_2 is the duty cycle of part II; L_1 and L_2 are the inductances of first and second stage, respectively; i_{L1} and i_{L2} are the currents of L_1 and L_2, respectively; C_1 and C_2 are the capacitances of the first and second stage, respectively; V_{c1} and V_{c2} are the voltage of C_1 and C_2, respectively; R_L is the back-end load; V_{PV} is the voltage of the PV array, which is also specified and related to i_{PV}, as shown in Eq. (1). i_{L1} is equal to i_{PV} defined in Eq. (1). Taking the time averages of state-space variables, the capacitance voltages and inductance currents in Eqs. (2–4), in a single duty-cycle period [i.e., the so-called "state-space averaging method" (Qian 2010)], the governing equations (2–4) can be further simplified as

$$\begin{bmatrix} \dot{i}_{L1}(t) \\ \dot{i}_{L2}(t) \\ \dot{V}_{C1}(t) \\ \dot{V}_{C2}(t) \end{bmatrix} = \begin{bmatrix} 0 & 0 & \frac{-(1-D_1-D_2)}{L_1} & 0 \\ 0 & 0 & \frac{1}{L_2} & \frac{-(1-D_1)}{L_2} \\ \frac{1-D_1-D_2}{C_1} & \frac{-1}{C_1} & 0 & 0 \\ 0 & \frac{1-D_1}{C_2} & 0 & \frac{-1}{R_L C_2} \end{bmatrix} \times \begin{bmatrix} i_{L1}(t) \\ i_{L2}(t) \\ V_{C1}(t) \\ V_{C2}(t) \end{bmatrix} + \begin{bmatrix} \frac{1}{L_1} \\ 0 \\ 0 \\ 0 \end{bmatrix} V_{PV}(t). \tag{5}$$

As for case II, where the duty cycle of Q_2 is longer than Q_1, the state-space governing equations are also derived herein. Following the same procedure, the state-space equations in the periods of D'_1 and $(1-D'_1-D'_2)$ are in the

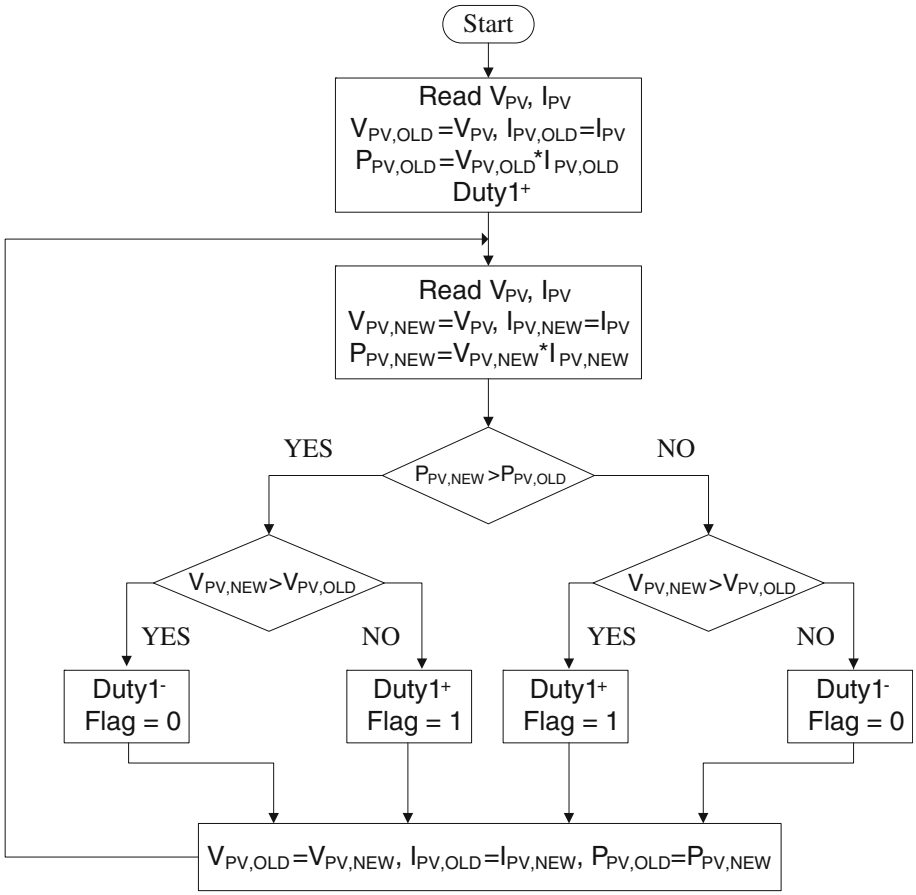

Fig. 5 The computation flow chart of the control algorithm (Zhong et al. 2008)

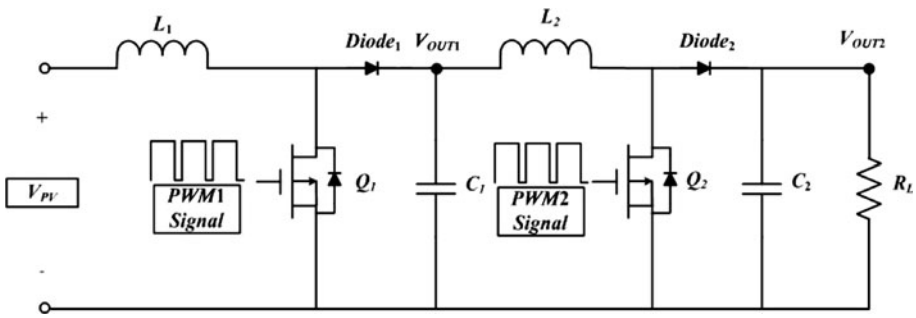

Fig. 6 The two-stage DC–DC converter circuit

same forms as Eqs. (2) and (4), respectively, while the equations for D'_2 can be expressed as

$$\begin{bmatrix} \dot{i}_{L1}(t) \\ \dot{i}_{L2}(t) \\ \dot{V}_{C1}(t) \\ \dot{V}_{C2}(t) \end{bmatrix} = \begin{bmatrix} 0 & 0 & \frac{-D'_2}{L_1} & 0 \\ 0 & 0 & \frac{D'_2}{L_2} & 0 \\ \frac{D'_2}{C_1} & \frac{-D'_2}{C_1} & 0 & 0 \\ 0 & 0 & 0 & \frac{-D'_2}{R_L C_2} \end{bmatrix} \begin{bmatrix} i_{L1}(t) \\ i_{L2}(t) \\ V_{C1}(t) \\ V_{C2}(t) \end{bmatrix} + \begin{bmatrix} \frac{D'_2}{L_1} \\ 0 \\ 0 \\ 0 \end{bmatrix} V_{PV}(t), \quad (6)$$

which is different from Eq. (3) in some signs of entries in the matrix associated with state variables. Employing the aforementioned state-space average method on the inductance currents and capacitance voltages prescribed in Eqs. (2, 4, 6), the governing equations for case II can be further simplified as

$$\begin{bmatrix} \dot{i}_{L1}(t) \\ \dot{i}_{L2}(t) \\ \dot{V}_{C1}(t) \\ \dot{V}_{C2}(t) \end{bmatrix} = \begin{bmatrix} 0 & 0 & \frac{-\left(1-D'_1\right)}{L_1} & 0 \\ 0 & 0 & \frac{1}{L_2} & \frac{-\left(1-D'_1-D'_2\right)}{L_2} \\ \frac{1-D'_1}{C_1} & \frac{-1}{C_1} & 0 & 0 \\ 0 & \frac{1-D'_1-D'_2}{C_2} & 0 & \frac{-1}{R_L C_2} \end{bmatrix} \times \begin{bmatrix} i_{L1}(t) \\ i_{L2}(t) \\ V_{C1}(t) \\ V_{C2}(t) \end{bmatrix} + \begin{bmatrix} \frac{1}{L_1} \\ 0 \\ 0 \\ 0 \end{bmatrix} V_{PV}(t). \quad (7)$$

With governing Eqs. (2–7) in hands, the system dynamics of each stage in the adopted two-stage converter can be successfully simulated with the controllers designed via aforementioned methods of P&O or FC-MPPTC.

2.3 Determining inductances and capacitances

With electrical dynamics captured by the governing equations derive in the last subsection, effort is dedicated to determine inductances and capacitances of the designed two-stage DC–DC converter. Design of a DC–DC boost converter is basically intended to elevate the original DC input to a steady output DC voltage (Esram and Chapman 2007). The designation of passive devices in this converter is carried out by first considering two equivalent circuits as shown in Fig. 8, two topologies of which refers to different cases with switch on and off. Following a standard procedure of analysis via the conversion between continuous and discrete representations of the inductance current, as given in (Esram and Chapman 2007), one can obtain the output voltage simply equal to

$$V_{OUT} = \frac{V_{IN}}{1 - D}, \tag{8}$$

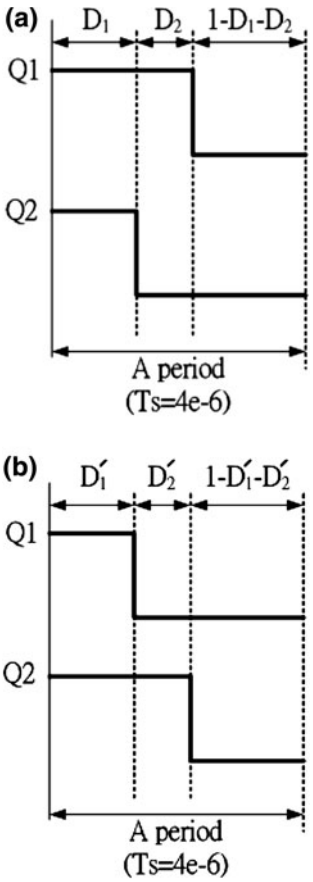

Fig. 7 The duty cycles of the two-stages in the DC–DC converter: **a** case I, **b** case II

where D is varied between [0.1, 0.9]. The output voltage is successfully boosted to a higher level. Figure 9a shows the waveforms of inductance voltages. The analysis thus far is based on the assumption that the inductance current is continuous. The inductance current in fact varies over a cycle, varying between a minimum value ($I_{L,MAX}$) and a maximum value ($I_{L,MIN}$), which can be expressed in terms of mean value and change as expressed in equation, that is,

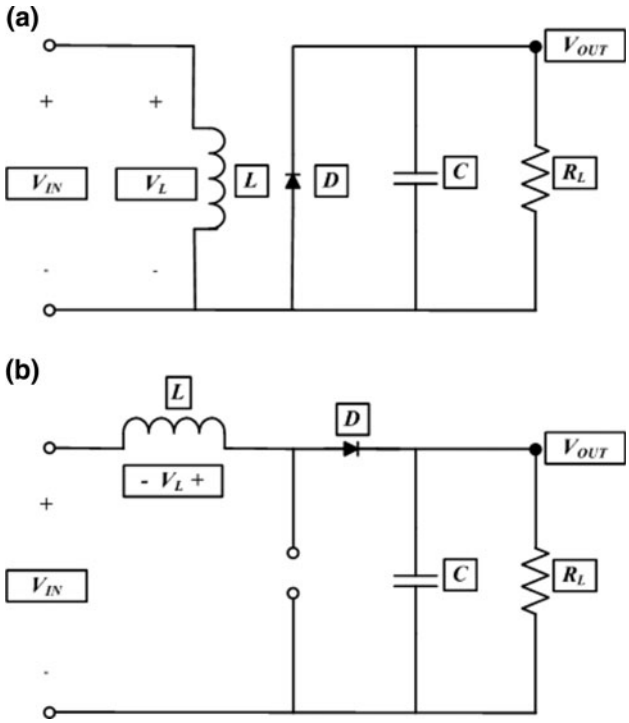

Fig. 8 **a** The equivalent circuit with the power switch closed; **b** The equivalent circuit with the power switch open

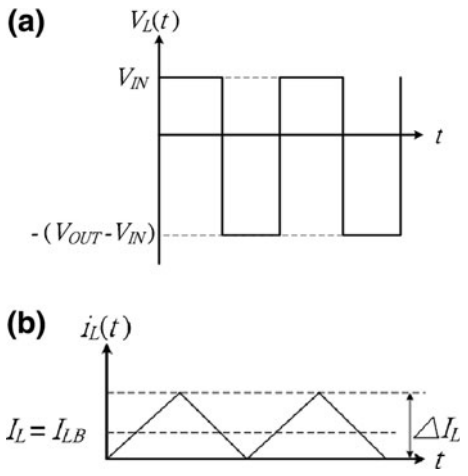

Fig. 9 **a** The waveform of the inductance current in a boost converter; **b** The inductance current boundary in a boost converter operated in continuous mode

$$I_{L,MAX} = I_L + \frac{\Delta I_L}{2}, \tag{9}$$

and

$$I_{L,MIN} = I_L - \frac{\Delta I_L}{2}, \tag{10}$$

where ΔI_L is the peak-to-peak current of the change value of inductance. Figure 9b shows that the maximum and minimum inductance currents can be obtained, for continuous conduction, as

$$I_L \geq \frac{\Delta I_L}{2}. \tag{11}$$

At the boundary of continuous and discontinuous conduction,

$$I_L = \frac{\Delta I_L}{2}. \tag{12}$$

Another expression for I_L is now obtained, i.e.,

$$I_L = \frac{V_{IN}}{(1-D)^2 \times R_L}, \tag{13}$$

where R_L is the load. Substituting for I_L from the equation above and for Δi_L from equation, equation becomes

$$I_{L,MAX} = \frac{V_{IN}}{(1-D)^2 \times R_L} + \frac{DT_s V_{IN}}{2L}, \tag{14}$$

and

$$I_{L,MIN} = \frac{V_{IN}}{(1-D)^2 \times R_L} - \frac{DT_s V_{IN}}{2L}, \tag{15}$$

where T_s is the sampling period. From Eqs. (14) and (15), the conditions for continuous conduction is

$$L > \frac{DT_s}{2} \times (1-D)^2 \times R_L. \tag{16}$$

Consider L_1 and L_2 as the two inductances in the two stages of the DC–DC converter adopted in this study. Application of Eq. (16) for L_1 and L_2 leads to

$$L_1 > L_{1B} = \frac{D_1 T_s}{2} \times (1-D_1) \times \frac{V_{PV}}{I_{OUT1B}} \tag{17}$$

$$L_2 > L_{2B} = \frac{D_2 T_s}{2} \times (1-D_2)^2 \times \frac{V_{OUT2}}{I_{OUT2B}} \tag{18}$$

where V_{PV} is the output voltage of the PV array; L_{1B} and L_{2B} are the critical inductances between CCM and DCM for the first and second stages, respectively; I_{out1B} and I_{out2B} are the critical output currents between CCM and DCM for the first and second stages, respectively; D_1 and D_2 are the duty cycles for the first stage and second stage, respectively. Utilization of the resulted Eqs. (17) and (18) gives the final designated inductances in the converter circuit adopted in this study. For the PWM design used for the current study, T_s is equal to 40 μs; I_{out1B} is equal to 0.5 A and V_{PV} is from 50 to 130 V. Considering the minimum critical inductance for CCM, V_{PV} is chosen with 130 V, while D_1 is chosen as 0.5. L_1 can be then calculated by Eq. (17) with these parameters as

$$L_1 > \frac{0.5 \times 40 \times 10^{-6} \times (1-0.5) \times 130}{2 \times 0.5} = 1{,}300\,\mu\text{m}. \tag{19}$$

Similarly, when the maximum output voltage of second stage ($V_{OUT2,MAX}$) equals to 300 V, T_s is equal to 40 μs; I_{out2B} is equal to 0.45 A; and D_1 is chosen as 0.5, L_2 can be calculated by Eq. (18) with these parameters as

$$L_2 > \frac{0.5 \times 40 \times 10^{-6} \times (1-0.5)^2 \times 300}{2 \times 0.45} \cong 1{,}667\,\mu\text{H}. \tag{20}$$

The focus of analysis is now turned to determine two capacitances in each of the two stages in the entire converter circuit. It is known based on fundamental principles that the system output capacitance C_2 in Fig. 6 dictates the level of the peak-to-peak ripple in the output voltage, which are for most cases supposed to be contained. When the switch Q_2 is closed, the output voltage is sustained by the capacitance C_2 in Fig. 6. During this period, the capacitance discharges part of its stored energy and it re-acquires this energy when the switch is open. When the switch is open, part of the inductance current charges the capacitance since the inductance current usually remains larger than the current through the load resistor, leading to

$$i_{c2}(t) = C_2 \frac{dV_{OUT2}(t)}{dt}, \tag{21}$$

when the capacitance current i_{c2} is constant, the voltage changes linearly with time. Here the period for which the switch is closed is D_2T_s, D_2T_s is denoted herein by Δt. The peak-to-peak ripples in the output voltage denoted by ΔV_{OUT2} (Mohan et al. 2003) can then be derived as

$$\Delta V_{OUT2} = \frac{i_{c2} \times (D_2 T_s)}{C_2} = \frac{I_{OUT2} D_2 T_s}{C_2}, \tag{22}$$

where I_{OUT2} is the output current of the second stage. Similarly, ΔV_{OUT1} can then be derived as

$$\Delta V_{OUT1} = \frac{i_{c1} \times (D_1 T_s)}{C_1} = \frac{I_{OUT1} D_1 T_s}{C_1}, \tag{23}$$

where I_{OUT1} is the output current of the first stage. Based on Eqs. (22) and (23), the capacitances C_1 and C_2 can be determined by

$$C_1 = \frac{I_{OUT1} D_1 T_s}{\Delta V_{OUT1}} = \frac{I_{PV}(1-D_1) D_1 T_s}{\Delta V_{OUT1}}, \tag{24}$$

$$C_2 = \frac{I_{OUT2} D_2 T_s}{\Delta V_{OUT2}} = \frac{I_{OUT1}(1 - D_2) D_2 T_s}{\Delta V_{OUT2}}, \quad (25)$$

where I_{PV} is the output current of solar array; ΔV_{OUT1} and ΔV_{OUT2} are the peak-to-peak ripples in the output voltages for the first and second stage, respectively. I_{OUT1} is the output current of the first stage. Considering that I_{PV} is equal to 5 A, T_s is equal to 40 μs, D_1 is equal to 0.5 and ΔV_{OUT1} is equal to 0.5 V, Eq. (24) offers the design of C_1 as

$$C_1 = \frac{5 \times (1 - 0.5) \times 0.5 \times 40 \times 10^{-6}}{0.5} = 100\,\mu\text{F}. \quad (26)$$

Considering that I_{OUT1} is equal to 4.5 A, T_s is equal to 40 μs, D_2 is equal to 0.5 and ΔV_{OUT2} is equal to 0.5 V, Eq. (25) offers the design of C_2 as

$$C_2 = \frac{4.5 \times (1 - 0.5) \times 0.5 \times 40 \times 10^{-6}}{0.5} = 90\,\mu\text{F}. \quad (27)$$

To this point, all the passive components of the design two-stage PV system are successfully determined and listed in Table 1. The determined inductances and capacitances would be later used for realizing the two-stage DC–DC converter.

3 Design of fuzzy controller

An MPPT is designed and applied to the switch in the first stage for arbitrary irradiation level and temperature, which is the main objective of the FC-MPPTC proposed in this study. On the other hand, a basic voltage boost controller (VBC) is adopted for the second stage. This VBC employs a fundamental voltage feedback control, as a PI controller. The goal of VBC is to boost the output voltage above the operable voltages of the back-end electronics (SMA sunny boy 4000TL) where the operating voltage rang is required to be from 125 to 440 V. The design of the FC-MPPTC for the first stage is elaborated as follows by the three parts—fuzzification, interference rules and defuzzification.

Table 1 The designed values of the components of the PV system

L_1	1.5 mH	$R_{P\text{-}PV1}$	22 KΩ
L_2	2 mH	$R_{P\text{-}PV2}$	150 KΩ
C_1	220 μF	$R_{P\text{-}PV3}$	22 KΩ
C_2	220 μF	$R_{P\text{-}PV4}$	150 KΩ
$R_{OUT2.1}$	50 KΩ	R_{PV1}	470 KΩ
$R_{OUT2.2}$	470 Ω	R_{PV2}	10 KΩ
R_{G1}	150 Ω	R_{PV3}	50 KΩ
R_{G2}	1.5 KΩ	R_{PV4}	1 KΩ
R_{G3}	150 Ω	R_L	10 Ω
R_{G4}	1.5 KΩ	R_{HY}	1 KΩ

3.1 Fuzzification

The first phase of computation for a fuzzy controller is fuzzification, which is started with choosing the output voltage (V_{PV}) and power (P_{PV}) of the PV array as the two input variables of the fuzzy controller to be designed, since the PV voltage is adjusted to reach maximum power during MPPT. The adjustment increment on V_{PV} is tuned based on the instantaneous value of P_{PV}. In this way, two sets of membership functions are defined for variations of the output voltage (denoted by ΔV) and power (denoted by ΔP) of the PV array, respectively, as shown in Fig. 10. On the other hand, the output of the controller is the variation on duty cycle of the switch (denoted by$\Delta\hat{D}$) for the first stage of the converter. The fuzzification on the aforementioned input and output variables next carried out by five fuzzy sets as NB, NS, ZE, PS, PB in the same triangle membership functions as

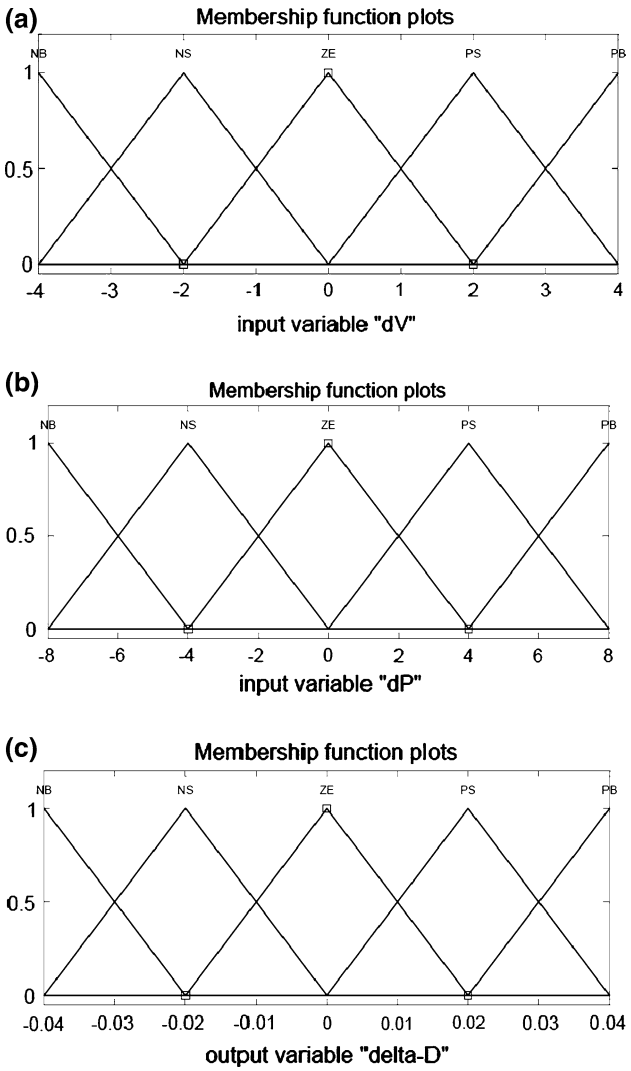

Fig. 10 The membership functions of **a** voltage variation; **b** power variation; **c** output duty cycle variation

shown in Fig. 10. The range for input ΔV is chosen from -4 to 4. The range for input ΔP is defined from -8 to 8. The range for output $\Delta\hat{D}$ is defined from -0.04 to 0.04.

3.2 Fuzzy rule base and fuzzy inference

With memberships defined, linguistic rules for the fuzzy controller are determined based on the rules in fact equivalent to those described in Fig. 5 for the aforementioned P&O method. This would lead the operating point of the PV array to approach the maximum power point. Even with the same linguistic rules, the FC-MPPTC controller proposed herein is considered more advanced than the conventional P&O method due to its capability to continuously tune the level of duty increment via the mechanism of fuzzification, interference and defuzzification. The IF–THEN rules of fuzzy control for the four conditions following the flow chart of control algorithm in Fig. 5 could be expressed as

$$IF\ \Delta P<0 \quad and \quad \Delta V<0,\ THEN\ \Delta\hat{D}<0; \tag{28}$$

$$IF\ \Delta P<0 \quad and \quad \Delta V>0,\ THEN\ \Delta\hat{D}>0; \tag{29}$$

$$IF\ \Delta P>0 \quad and \quad \Delta V<0,\ THEN\ \Delta\hat{D}>0; \tag{30}$$

$$IF\ \Delta P>0 \quad and \quad \Delta V>0,\ THEN\ \Delta\hat{D}<0. \tag{31}$$

The associated rule table is shown in Table 2, which enables a continuous, smooth adjustment on the duty increment $\Delta\hat{D}$.

3.3 Defuzzification

Having forged fuzzy interference scheme, linguistic output variables need to be converted into numerical values. The subsequent defuzzification is carried, which is in fact an inverse transformation of fuzzification. It maps the output from the fuzzy domain back into the numerical domain. The center average method is used herein for defuzzification, which could be expressed as

$$\Delta\hat{D}=\frac{\sum_{i=1}^{4} W_i\times\Delta D}{\sum_{i=1}^{4} W_i}, \tag{32}$$

where W is the height of fuzzy set and ΔD is the center of area of fuzzy set.

Table 2 Fuzzy rule table

dP	dV				
	NB	NS	ZE	PS	PB
NB	NB	NB	NB	PB	PB
NS	NS	ZE	ZE	ZE	PS
ZE	NS	ZE	ZE	ZE	PS
PS	PS	ZE	ZE	ZE	NS
PB	PB	PB	PB	NB	NB

4 Simulation and experiments

With system models established and controllers deigned, simulations and experiments are conducted to tune controller parameters and validate the expected performances of simultaneous MPPT by the first stage and boosting the output voltage to a required higher level by the second stage.

4.1 Simulation results

The dynamics of the state-space equations (5) and (7) is simulated by a MATLAB program. The results are compared with those by Powersim. The system description for the circuit simulation carried out by Powersim is shown in Fig. 11. The input voltage is 21 V, L_1 is 1.5 mH, L_2 is 2 mH, C_1 and C_2 are both 220 μF, R_L is 10 Ω. Note that these passive components are chosen satisfying design criteria distilled by Eqs. (19–20) and (26–27). The comparison between the results of state-space and Powersim simulation are shown in Table 3, where two conditions are considered: (1) the duty of the first stage is longer than second one and (2) duty of the first stage is shorter than second one. It is seen form the results given in this table that the state-space equations render results very close to those by Powersim. This verifies the correctness of the established state-space equations.

The afore-mentioned P&O and designed FLC algorithms are realized and embedded into the block DLL in this figure by C language. Comparison is made between the methods of P&O and FLC in term of performance in MPPT. Figure 12 presents varied simulation results by governing equations or Powersim for MPPT, where the Siemens solar module SP75 is considered. The corresponding MPP is at 74.8 Watt with V_{MPP} in 17 V and I_{MPP} in 4.4 A. Note that since the resulted simulation results by state-space equations and Powersim are distinguishable if presented in the figure, only the results from Powersim are plotted as the representative simulation results. It is seen from this figure that MPP is reached within a short period of 0.02 s. Also, much more oscillation occurs for the case with the P&O method employed, not only in transient but also in the steady state period. On the contrary, the designed FLC could track the MPP in a faster pace with high precision. In a short conclusion, the simulation results show that the proposed FC-MPPTC with the designed two-stage converter and the PV system could track the MPP efficiently and effectively.

4.2 Experimental validation

4.2.1 Experimental setup

An experiment system as shown in Fig. 13 is established for validating the expected performance of controllers and

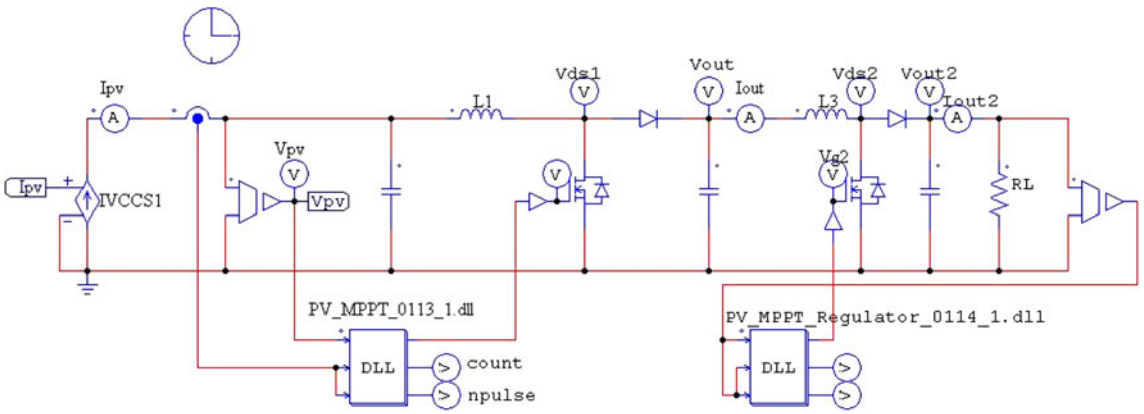

Fig. 11 The circuit model established by Powersim

Table 3 Simulation result based on state space and Powersim model

	Condition (1)				Condition (1)			
	The duty of the first stage is longer than second one				The duty of the first stage is shorter than second one			
D_1	0.1	0.2	0.3	0.4	0.5	0.6	0.7	0.8
D_2	0.2	0.4	0.6	0.8	0.4	0.2	0.3	0.5
V_{out} (*State space*)	29.17	43.74	74.98	174.7	70	65.61	99.96	209.6
V_{out} (*Powersim*)	29.165	43.745	74.977	174.718	69.984	65.612	99.959	209.626

the two-stage DC–DC converter. It includes a 32-bit microprocessor of DSP (TI TMS320F2812), an optical coupler circuit and a current sensor (HY-10P). The aforementioned DSP chip (TMS320F2812) is a stand-alone module which features a 150 MHz clock, a high-performance 32-Bit processor, and 12-bit ADC output. The optical coupler is an isolating device consisting of a transmitter and a receiver, through which the electrical signal is converted to a light beam, transferred, then converted back to an electrical signal. In this way, electromagnetic interference and undesired electrical pulsations could be isolated to the DSP module. Note that an optical isolator is usually regarded as a single integrated package, but the opto-isolation can also be achieved by using separate devices. Digital opto-isolators modify the state of their outputs when the input state changes. Analog isolators produce an analog signal which reproduces the input. Figure 14 shows the circuit insight of the isolated gate driver. In addition, the diode (1N5819) improves the falling time with the optical coupler, which accelerates the charge into ground. Finally, the hall current sensor (HY-10P) is used to sense the electrical current from the photovoltaic panels. Figure 15 shows the schematic of the hall sensor that connects the resistance from the output of HY-10P into ground and in a parallel fashion with a zener diode to limit the output voltage under 3 V. This avoids the breakdown of the analog to digital channel (ADC) of DSP (TMS320F2812). Table 4 lists the currents converted to the voltage for ADC sensing.

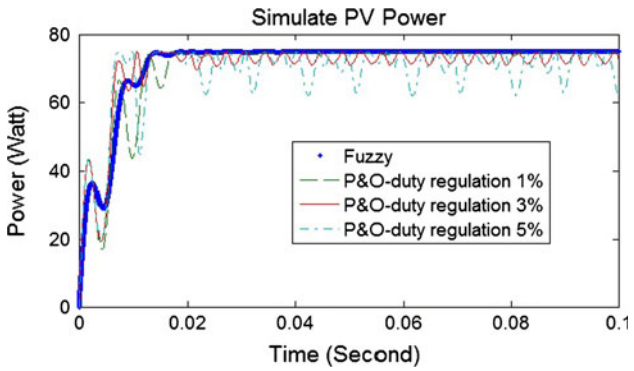

Fig. 12 Simulation results of the output power of the PV array with P&O method and FLC

The voltage and current of the PV module are sensed by an optical coupler circuit and a current sensor, respectively. The sensed signals of voltage and current are used as the inputs to the FC-MPPTC. One particular realistic design of the circuit is that if the voltage of the PV array is higher than the back-end operation of the inverter voltage, the voltage of PV array would be passed via switch $Q_{P\text{-}PV1}$ to drive the back-end inverter. The corresponding by-pass loop is also shown in Fig. 13 on the top portion of the entire circuit. On the other hand, the switch $Q_{P\text{-}PV1}$ is off,

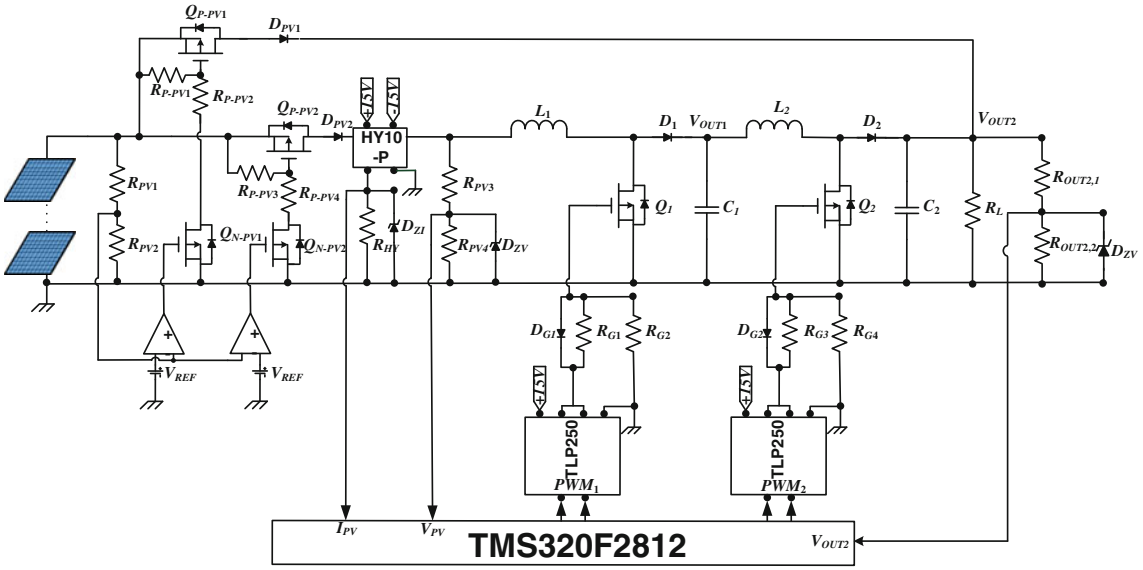

Fig. 13 The designed two-stage photovoltaic and converter system

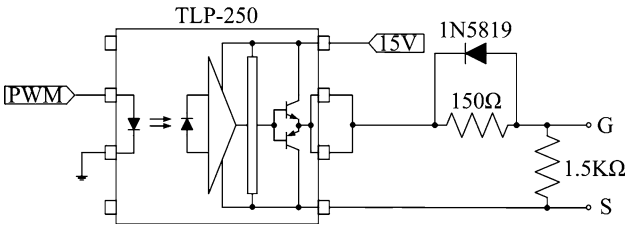

Fig. 14 The schematic of the isolated gate driver circuit

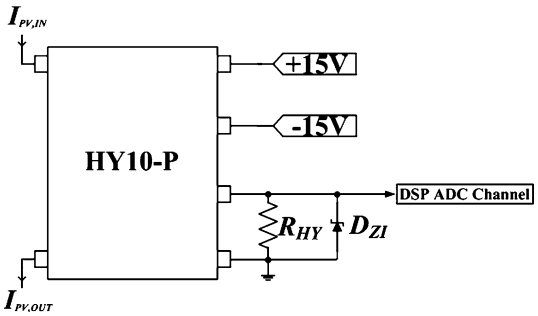

Fig. 15 The schematic of the hall current sensing circuit

when the voltage of the PV array needs to be boosted to the operating voltage of inverter.

Figure 16 gives a photo showing the implementation of the designed circuit for the two-stage DC–DC converter.

Figure 17 shows the entire testing system, where a photovoltaic (PV) panel is replaced by the Agilent Solar Array Simulator (E4362A), which is a 600 W PV simulator, and a direct-current power module that simulates the output characteristics of a photovoltaic (PV) string. This E4362A is in fact a current source with a low output capacitance that offers current–voltage curve changes to allow users to accurately simulate the output of different PV strings under various environmental conditions. Four key operational parameters (V_{OC}, I_{SC}, V_{MP}, I_{MP}) are needed for the PV simulator to create a characteristic curve of a PV string. V_{OC}, I_{SC}, V_{MP} and I_{MP} are open-circuit voltage, short-circuit current, voltage at MPP and current at MPP, respectively.

4.2.2 Experiment results

Figure 18 shows the experiment results by setting the open circuit voltage V_{oc} of the PV-string simulator E4362A at 130 V, short circuit current I_{sc} 3 A, maximum power voltage V_{MP} 110 V and the maximum power current I_{MP} 2A. Figure 18a is the interface of the Agilent web control, which is provided by the simulator E4362A, where is seen for this case an I–V curve of a PV panel. The red point is the instantaneous operating point of the PV array in terms of current and voltage. With the designed FC-MPPTC controller implemented by the DSP module and in operation, the operating point (red dot) is successfully stabilized

Table 4 Measurements by the hall current sensor

I_{PV} (A)	0.5	1	1.5	2	2.5	3	3.5	4	4.5	5	5.5	6
V_{ADC} (V)	0.190	0.390	0.580	0.780	0.985	1.186	1.386	1.581	1.781	1.973	2.163	2.363

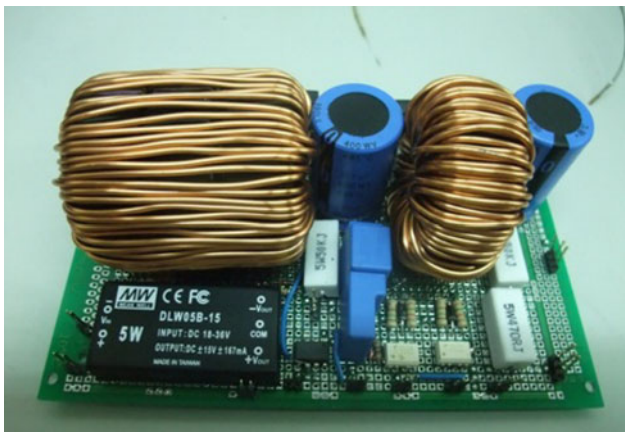

Fig. 16 The implemented designed circuit

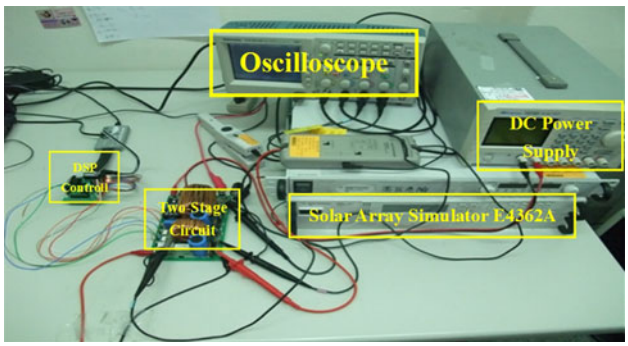

Fig. 17 Experimental Setup

after some period of time to the MPP. The stabilization evolution is shown in Fig. 18b. It is seen from this subfigure that with the DSP module power on (the controller on), the output power is maximized to approximate 220 W in a time period around 13 s, when the current and voltage of the PV panel reaches 2 A and 110 V, respectively, actually corresponding to the location of the red dot in Fig. 18a. Note that the 13 s is much longer that the stabilizing time period of 0.02 s simulated by governing equations or Powersim, as previously shown in Fig. 12, since in experiments the MPPT is activated intermittently with 1 s rest each time between two successive duty adjustment. For this case of MPPT, only 13 times of adjustments are needed to reach MPPT. Except the rest time, the actual operation period needed for MPPT is less than 1 s, showing a fast MPPT achieved by the designed FC-MPPTC controller.

Note also that noises are observed in various signals which are possibly resulted from ADC and/or environment.

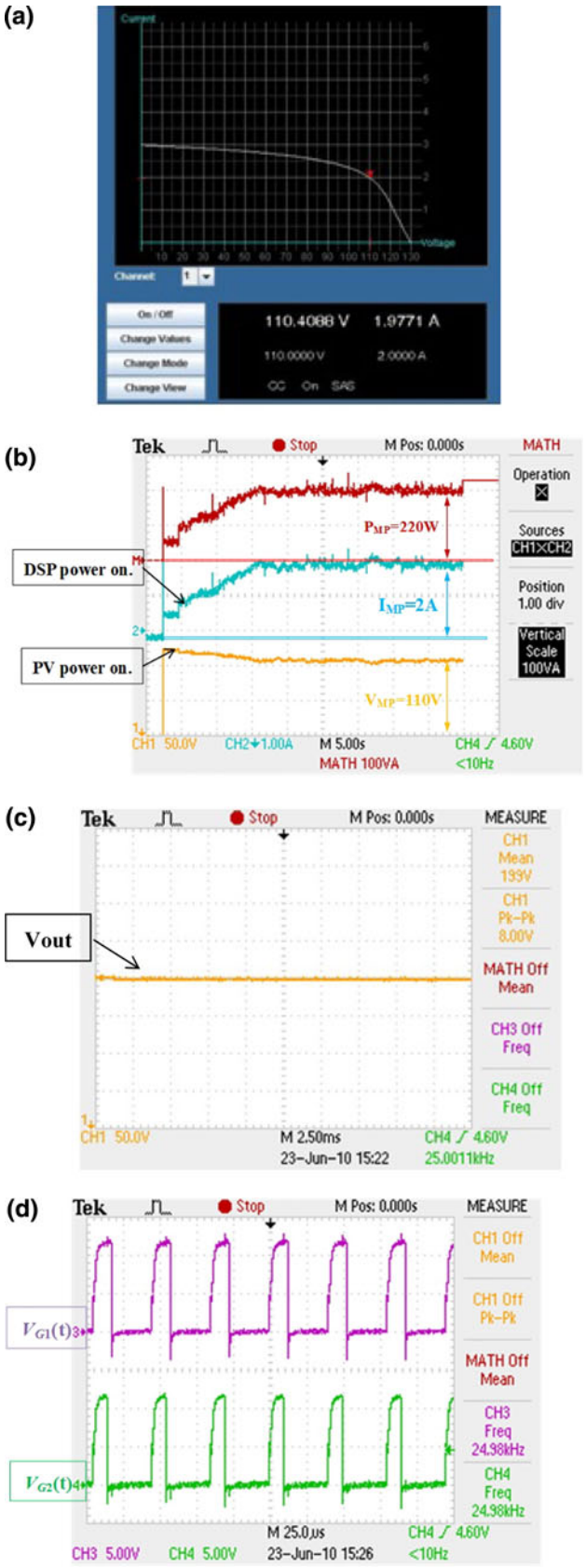

Fig. 18 Experimental results by the PV simulator (V_{OC} = 130 V, I_{SC} = 3 A, V_{MP} = 110 V, I_{MP} = 2 A); **a** Agilent web control; **b** Waveforms (V_{PV}, I_{PV}, P_{PV}); **c** Output voltage waveforms in the second stage; **d** The duties of two-stage converter ▶

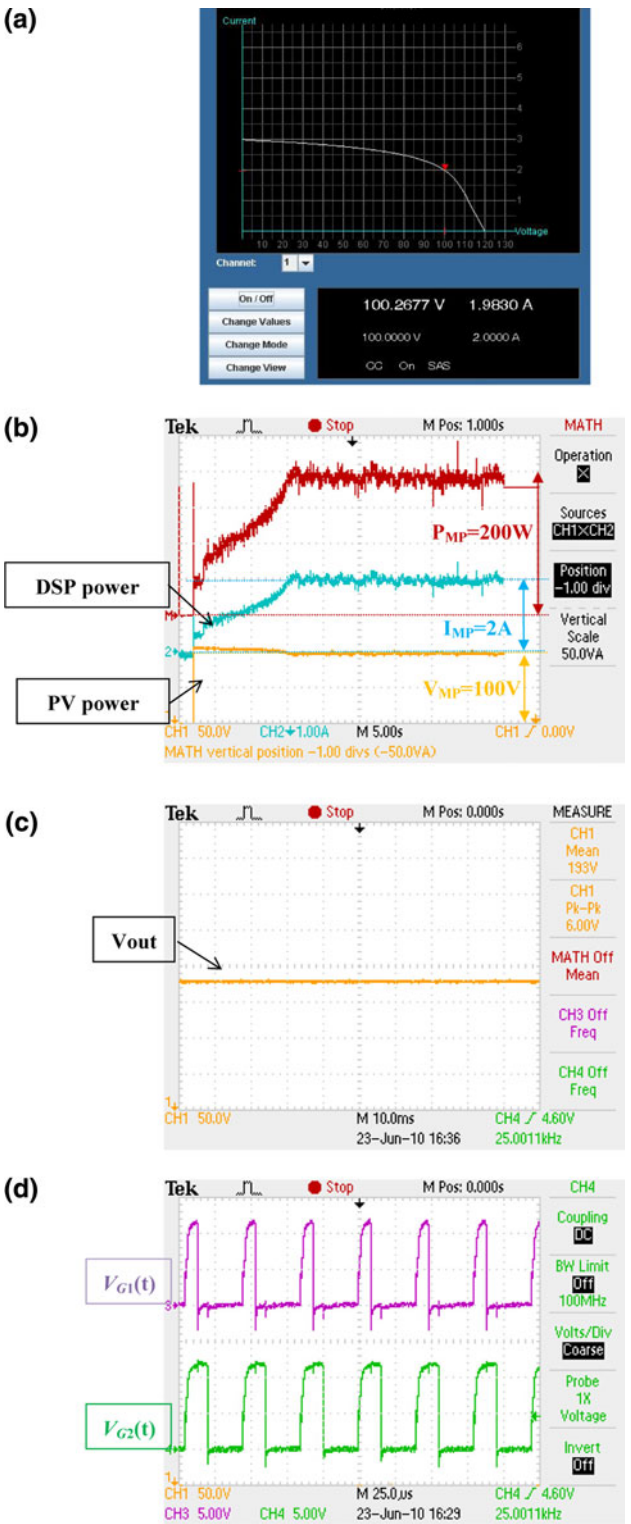

Fig. 19 Experimental results by the PV simulator (V_{OC} = 120 V, I_{SC} = 3 A, V_{MP} = 100 V, I_{MP} = 2 A); **a** Agilent web control; **b** Waveforms (V_{PV}, I_{PV}, P_{PV}); **c** Output voltage waveforms in the second stage; **d** The duties of two-stage converter

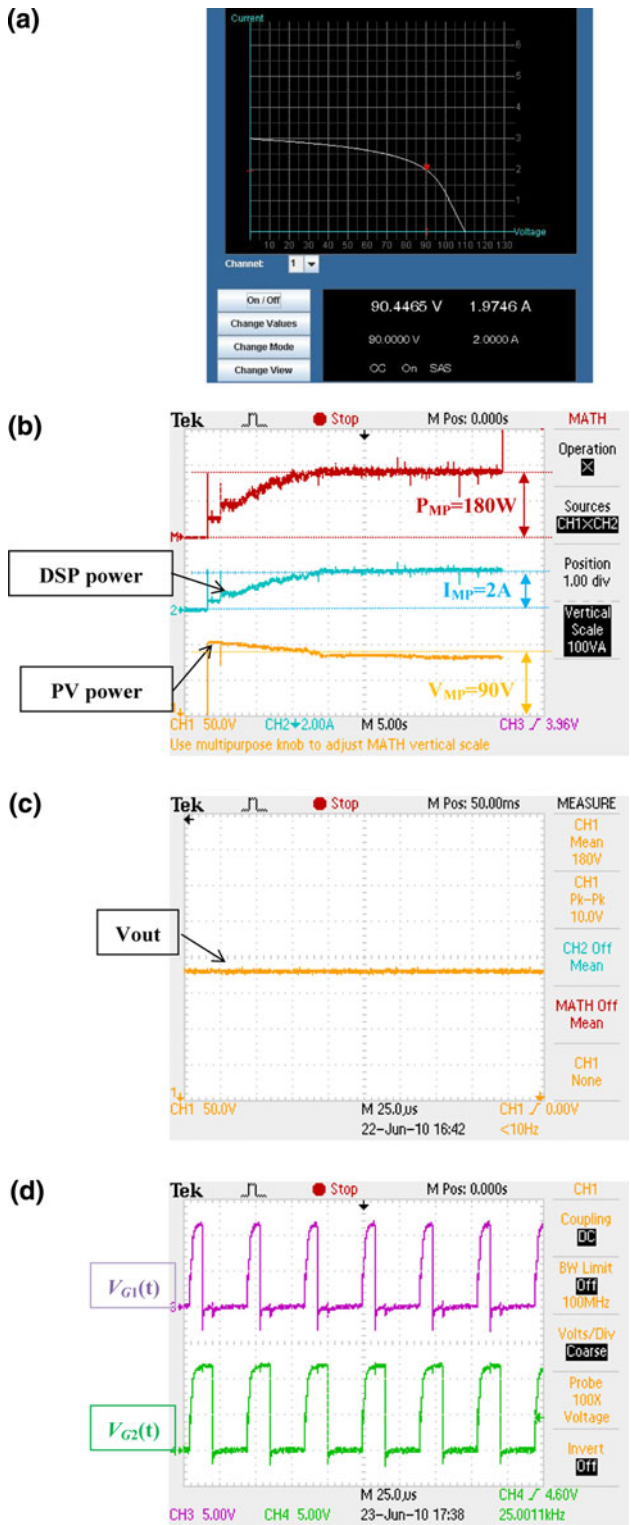

Fig. 20 Experimental results by the PV simulator (V_{OC} = 110 V, I_{SC} = 3 A, V_{MP} = 90 V, I_{MP} = 2 A); **a** Agilent web control; **b** Waveforms (V_{PV}, I_{PV}, P_{PV}); **c** Output voltage waveforms in the second stage; **d** The duties of two-stage converter

Figure 18c shows the output voltage waveforms of the second stage in the adopted DC-C converter, where the value of the output voltage is stabilized at 199 V, showing the capability of the designed controller and circuit topology to provide a constant output and maximum power output from the PV panel. The waveforms of the duties in the two stages are shown in Fig. 18d. The duty cycle of first stage and second stages are approximately equal to 32.3 and 23.5 %, respectively, at MPP. The required time for stabilizing at MPP is approximately equal to 11 s to reach the maximum power point.

The performance of the designed FC-MPPTC controller and the two-stage converter topology are also tested for different I–V characteristics of the PV module. Their simulation results similar to the previous case are shown in Figs. 19 and 20, where V_{oc} of the PV-string set lower as 120 and 110 V, respectively. With the designed FC-MPPTC controller in operation, both PV panels are stabilized at their MPPs successfully within 13 s. The voltages at MPPs V_{MP}'s are 100 and 90 V, respectively, for the two cases. The final duties in the two stages in Fig. 19d for the case with V_{oc} = 120 V equal to approximately 23.5 and 38.2 %, respectively, the final duties in the two stages in Fig. 19d for the case with V_{oc} = 110 V approximately equal to 20.5 and 41.1 %, respectively. Therefore, when V_{MP} becomes low, the duty for the second stage is tuned to a higher level, while the first one to a lower level. It is obvious that the tunings on the duties for the two different stages in the DC–DC converter while the maximum power tracking is in action by the designed FC-MPPTC controller are actually heading toward opposite direction.

Much effort is next paid to collect experimental data on the powers at different stages, which is intended to compute the conversion power efficiencies of the designed circuit. Varied trails of MPPT for different I–V characteristics of the PV panel are carried out. The results are summarized in Table 5. In this table, P_{OUT1} is the realistic power output of the PV simulator measured at the output of the first-stage, which is supposed to be ideally equal to P_{MP} at steady state while MPPT is effective. The difference between shown in this table reflects inevitable power losses, like switching and conduction losses. V_{OUT2} and P_{OUT2} are the output voltage and power of the second stage in the adopted two-stage DC–DC converter. Two efficiencies are defined to further evaluate the performance of the designed FC-MPPTC controller and DC–DC converter. They are defined by

$$\eta_{2nd-stage} = \frac{P_{OUT2}}{P_{OUT1}}, \tag{33}$$

$$\eta_{system} = \frac{P_{OUT2}}{P_{MP}}. \tag{34}$$

The above-defined two efficiencies $\eta_{2nd-stage}$ and η_{system} in fact refers to those of the 2nd-stage converter and the entire system. It is seen from Table 5 that the system conversion efficiency varies from 90 to 96.302 %, which all above 90 %, showing satisfactory energy conversion results of the designed FC-MPPTC controller and DC–DC converter. The best efficiency is obtained for the case with V_{OC} and I_{SC} being 130 V and 3 A, respectively, for the I–V characteristics of the PV panel.

5 Conclusion

A new two-stage DC–DC converter equipped fuzzy tracker for maximum power point tracking (MPPT) and simultaneous voltage boost of a generic PV system is proposed in this study. Modeling and simulation on the PV system and the DC–DC converter circuit are carried out by the state-space technique and the software Powersim. The simulations are intended to validate the performance of the proposed FC-MPPTC. It is shown that the tracking process for the maximum power point is as fast as within 0.02 s, which is also proven in a much faster pace and stable with designed FC-MPPTC as compared to conventional P&O method. Experiments are also carried out to validate the expected performance of the designed FC-MPPTC

Table 5 Measured powers for tuning duties of the two switches in the two stages

V_{oc} (V)	I_{sc} (A)	V_{MP} (V)	I_{MP} (A)	P_{MP} (W)	P_{out1} (W)	V_{out2} (V)	P_{out2} (W)	$\eta_{2nd\text{-}stage}$ (%)	η_{system} (%)
130	3	120	2	240	234.611	215	231.125	98.514	*96.302*
130	3	110	2	220	218.289	199	198.005	90.708	90.002
130	3	100	2	200	198.167	195	190.125	95.942	95.063
120	3	110	2	220	219.243	200	200.000	91.223	90.909
120	3	100	2	200	198.831	193	186.245	93.670	93.123
120	3	90	2	180	178.751	183	167.445	93.675	93.025
110	3	100	2	200	199.702	194	188.180	94.230	94.090
110	3	90	2	180	178.596	180	162.000	90.707	*90.000*

Italicized values represent the minimum and maximum possible efficiencies obtained from the experiment results

controller and the two-stage DC–DC converter. It is shown that a fast MPPT is achieved within less than 1 s, while the efficiency could reach more than 90 %, even up to 96.302 %, with varied conditions on the I–V characteristics of the PV cell considered. In short, the designed two-stage PV system with proposed FC-MPPTC and VBC is proven working effectively in extracting power from a generic photovoltaic system.

Acknowledgments The authors are greatly indebted to AU Optronics Corp. (AUO) for the supporting research. The authors also appreciate the support from National Science Council of R.O.C under the grant no. NSC 101-2623-E-009-006-D and 100-2221-E-009-091-. This work was also supported in part by the UST-UCSD International Center of Excellence in Advanced Bio-Engineering sponsored by the Taiwan National Science Council I-RiCE Program under Grant NSC-100-2911-I-009-101.

References

Agorreta JL, Reinaldos L, Gonzalez R, Borrega M, Balda J, Marroyo L (2009) Fuzzy switching technique applied to PWM boost converter operating in mixed conduction mode for PV systems. IEEE Trans Indus Electron 56(11):4363–4373

Al-Atrash H, Batarseh I, Rustom K (2005) Statistical modeling of DSP-based Hill-climbing MPPT algorithms in noisy environments. APEC 3:1773–1777

Bouchafaa F, Hamzaoui I, Hadjammar A (2011) Fuzzy logic control for the tracking of maximum power point of a PV system. Energy Procedia 6:633–642

Chiu CS (2010) T-S Fuzzy maximum power point tracking control of solar power generation systems. IEEE Trans Energy Convers 25(4):1123–1132

Esram T, Chapman PL (2007) Comparison of photovoltaic array maximum power point tracking techniques. IEEE Trans Energy Convers 22(2):439–449

Gao Lijun (2009) Parallel-connected solar PV system to address partial and rapidly fluctuating shadow conditions. IEEE Trans Indus Electron 56:1548–1556

Hua Ch, Lin J, Shen Ch (1998) Implementation of a DSP-controlled photovoltaic system with peak power tracking. IEEE Trans Indus Electron 45(1):99–107

Hussein KH, Muta I, Hoshino T, Osakada M (1993) Inductive energy storage for photovoltaic power systems. In: Proceedings of Technical digest of the Int'l PVSEC-7, Nagoya, Japan, pp 487–488

Jiang J-A, Huang T-L, Hsiao Y-T, Chen C-H (2005) Maximum power tracking for photovoltaic power systems. Tamkang J Sci Eng 8(2):147–153

Kottas TL, Boutalis YS, Karlis AD (2006) New maximum power point tracker for PV arrays using fuzzy controller in close cooperation with fuzzy cognitive networks. IEEE 21(3):793–803

Kwon JM, Nam KH, Kwon BH (2006) Photovoltaic power conditioning system with line connection. IEEE Trans Indus Electron 53(4):1048–1054

Mohan N (1995) Power electronics: converters, applications, and design. Wiley, New York, pp 63–101

Mohan N, Undeland TM, Robbins WP (2003) Power electronics, converters, applications and design, 3rd edn. Willey, Chichester

Qian Z (2010) Modeling and control of three-port DC/DC converter interface for satellite applications. IEEE Trans Power Electron 23:637–649

Salah CB, Ouali M (2011) Comparison of fuzzy logic and neural network in maximum power point tracker for PV systems. Electric Power Syst Res 81:43–50

Santos LJL, Antunes F, Chehab A, Cruz C (2006) A maximum power point tracker for PV systems using a high performance boost converter. Sol Energy 80(7):772–778

SMA Solar Technology (2010) Sunny Boy 4000TL Data Manual. http://www.solaraccess.co.uk/resources/invertor/datasheets/SB4000_5000TL-DEN090920_EN.pdf. Accessed 1 Sept 2010

Wasynczuk O (1983) Dynamic behavior of a class of photovoltaic power systems. IEEE Trans Power Apparatus Syst 102(9):3031–3037

Win KK, Dasgupta S, Panda SK (2011) An optimized MPPT circuit for thermoelectric energy harvester for low power applications. ICPE & ECCE 2011, pp 1579–1584

Xiao W, Dunford WG, Palmer PR, Capel A (2007) Regulation of photovoltaic voltage. IEEE Trans Indus Electron 54(3):1365–1374

Yuvarajan S, Yu D, Xu S (2004) A novel power converter for photovoltaic applications. J Power Sources 135(1–2):327–331

Zhong ZD, Huo HB, Zhu XJ, Cao GY, Ren Y (2008) Adaptive maximum power point tracking control of fuel cell power plants. J Power Sources 176(1):259–269